Limnol. Oceanogr., 48(1, part 2), 2003, 480–488

A remote sensing method for resolving depth and subpixel composition of aquatic benthos

John D. Hedley and Peter J. Mumby
Tropical Coastal Management Studies, Department of Marine Sciences & Coastal Management, Ridley Building, The University, Newcastle upon Tyne, NE1 7RU, Great Britain

Abstract

The problem of subpixel heterogeneity in cover types has been addressed in terrestrial environments by the application of linear spectral unmixing techniques. However, in aquatic systems the interceding depth of water causes the apparent reflectance of the substrate to diverge from a linear model, and if depth is unknown these methods cannot be applied. A new technique is presented in which the conventional spectral unmixing method has been modified to calculate depth at each pixel in addition to the proportions of substrate type. The technique requires knowledge of the reflectance spectra of m pure substrata in n ($n > m$) spectral bands at depth 0 and the water diffuse attenuation coefficients for the site in the same bands. Depth, z, can be entirely unknown. The method is comparable to ''classical'' spectral unmixing and proceeds by performing a Gaussian elimination for endmember quantities and then solving the remaining nonlinear function of z for $f(z) = 0$ by successive approximation. Computer-based models are used to test the technique with realistic water diffuse attenuation coefficients and random spectra and actual spectra of coral reef substrata. The robustness of the technique is assessed against three forms of introduced error: measurement errors on the spectra to be unmixed, differences between the true endmember spectra and those used in the analysis, and measurement error on the water diffuse attenuation coefficients. The results of these tests imply the technique is sufficiently robust for use on real data. Furthermore, spectral unmixing of aquatic systems appears to be relatively insensitive to inaccuracies in depth estimation and offers great utility for benthic mapping.

Remote sensing is widely used to map benthic substrata (reviewed by Green et al. 1996; Holden and LeDrew 1998) and bathymetry (Benny and Dawson 1983; Bierwirth et al. 1993) in aquatic systems. However, substrate reflectance and water depth are intimately associated and conventional analytical methods are unable to resolve one measure accurately unless the other is already known for each pixel. For example, if the water column diffuse attenuation coefficient (Maritorena and Guillocheau 1996) is known for each spectral band and the depth of each pixel has been measured independently, the at-surface reflectance of submerged substrata can be predicted, thus permitting spectral classification and benthic mapping (LeDrew et al. 1995; Mumby et al. 2001). In most practical situations, however, accurate bathymetric data are scarce (Bierwirth et al. 1993). This is particularly problematical in heterogeneous habitats such as coral reefs where a high spatial resolution is required (Green et al. 2000). Conversely, depth estimation requires an independent map of substrata or valid assumptions of an invariant substrate or bottom albedo. Depth estimation methods presented by Benny and Dawson (1983) and Jupp (1988) require a constant substrate, or at least a fairly constant albedo. Similarly, although the method of Bierwirth et al. (1993) does not rely on an invariant substrate, it does impose a constraint broadly equivalent to assuming the substrate is of uniform brightness. This results in darker benthos, such as seagrass, causing an erroneously large depth estimate. Nordman et al. (1990) described a method that requires the ratio of bottom reflectances in two or more bands to be constant, which is dependent on the substrata present and cannot be guaranteed. Lee et al. (2001) describe a method for simultaneously estimating various water column parameters including depth, but the method requires independent determination of the shape of the spectral reflectance of the substrate in each pixel. Lyzenga's (1978) method is based on taking the ratio of the natural logarithm of the signal in two bands and can be used to produce an index of depth. However, this index is the sum of a term dependent on depth and a term dependent on the absolute reflectance of the substrate in the two bands. To use this method effectively, the substrate must be identified for each pixel, and the depth indices for each substrate must be calibrated individually.

A second fundamental problem in remote sensing is the existence of substrate heterogeneity at subpixel scales (Mather 1999). This problem has been combated in terrestrial systems by spectrally unmixing the contribution of pure endmember spectra to each pixel, where each endmember is a substrate type (Adams et al. 1986; Foody and Cox 1994; Brown et al. 1999). Spectral unmixing makes the assumption that the measured spectral signal is the linear sum of a set of pure endmember spectra weighted by their relative abundance. Again, for an image of a submerged substrate, these methods cannot be applied unless the spectral signal can be depth corrected at every pixel. Adams et al. (1986) have demonstrated that shade effects can be removed by treating shadow as an endmember, and Peddle et al. (1995) have attempted a spectral mixture analysis on coral reefs where deep water was similarly treated as an endmember. However, water depth cannot be treated as a linear component in spectral mixing because the attenuation at any given wavelength

Acknowledgments

John Hedley is funded by the University of Newcastle. Peter Mumby is a Royal Society Research Fellow. The publication of the volume in which this article appears was supported by the Office of Naval Research Environmental Optics Program.

increases nonlinearly with depth, and the rate of this attenuation is dependent on wavelength.

The approach presented here solves the confounding influence of depth on substrate reflectance in the context of spectral unmixing. Depth and substrata can be unmixed providing that the spectra of all endmembers (at depth 0) are known together with the water column diffuse attenuation coefficients of each spectral band. In practice, both inputs can be derived from a brief field survey or estimated from spectral libraries and archived water quality data, respectively. Importantly, depth and substrata can be mapped without the need for extensive independent data.

Outline of the technique

The technique will be outlined both conceptually and mathematically in six stages. The first stage considers the model of light attenuation with depth, which forms the basis of the technique. Stage 2 reviews the principles behind linear spectral unmixing. Stage 3 describes the incorporation of light attenuation into the linear mixing model. Stage 4 describes, in principle, how the resultant model can be solved for depth, and stage 5 presents a practical technique by which this may be achieved. Finally, stage 6 describes an optional processing step based on principal components analysis (PCA), which can be used to increase efficiency of processing hyperspectral images when the number of bands greatly exceeds the number of endmembers.

The effect of depth on reflectance—Reflectance, as measured for remote sensing purposes, is loosely defined as the ratio of upwelling to downwelling radiation, although the strict definition is dependent on the field of view of the sensor(s) used (Kimes et al. 1980; Mobley 1994; Mather 1999). A material submerged under a depth of water will have an apparent reflectance that differs from its true (unsubmerged) reflectance due to the attenuation of light as it passes through the water column. The rate of attenuation varies with wavelength such that the apparent reflectance of a substrate at depth z in band i of a remotely sensed image, can be approximated as

$$R_z = R_0 e^{-2k_i z} \tag{1}$$

where R_0 is the reflectance of the substrate at depth zero and k_i is the diffuse attenuation coefficient for the water at the site at the wavelength of band i (Bierwirth et al. 1993). Strictly speaking, the downwelling and upwelling diffuse attenuation coefficients are distinct and defined in terms of depth, being denoted $K_d(z; \lambda)$ and $K_u(z; \lambda)$, respectively (Mobley 1994). However in practice, both coefficients often have nearly the same numerical values and depend only weakly on depth (Mobley 1994), so it is not uncommon for workers to use a single term for the diffuse attenuation coefficient, k (e.g., Bierwirth et al. 1993; Smith and Baker 1981). The values of k have been tabulated at 10-nm intervals between 200 and 800 nm for the clearest natural waters (Smith and Baker 1981), but in practice, these will vary from site to site, depending on the amount of suspended and dissolved material in the water. Additionally, this model ignores any surface specular reflection from the water or backscatter from within it. The former approximation is fair if we assume that the water surface is fairly flat and the angle of incident light and angle of measurement do not coincide. The technique presented here can be based on any model of apparent reflectance provided all the parameters other than depth can be characterized. In this instance, Eq. 1 was considered a reasonable approximation and is the basis of what follows.

Linear spectral unmixing—Linear spectral unmixing assumes that the multispectral signal received at a sensor is the sum of the spectral signals of one or more ''pure'' materials (or ''endmembers''), linearly proportional to their relative abundance in the sensor field of view (Mather 1999). In practice, this requires the solution of a set of n simultaneous equations of the form

$$\begin{aligned} r_1 &= a_{11}q_1 + a_{12}q_2 + \cdots + a_{1m}q_m \\ r_2 &= a_{21}q_1 + a_{22}q_2 + \cdots + a_{2m}q_m \\ &\vdots \quad\quad \vdots \quad\quad \vdots \quad\quad\quad \vdots \\ r_n &= a_{n1}q_1 + a_{n2}q_2 + \cdots + a_{nm}q_m \end{aligned} \tag{2}$$

where $r_1, r_2, \ldots, r_n$ represent the measured apparent reflectances of the pixels in n wavelength bands (in whatever units are being used), $q_1, q_2, \ldots, q_m$ are the quantities of m endmembers, expressed as proportions $0 \leq q_i \leq 1$. The a values represent the pure endmember spectra, such that the first subscript on a denotes the spectral band and the second denotes the endmember. Therefore, $a_{11}, a_{21}, \ldots, a_{n1}$ is the pure spectral signal of the first endmember (in the same bands and units as the r values), $a_{12}, a_{22}, \ldots, a_{n2}$ give the second pure endmember spectral signal and so forth.

Using matrices, this can be expressed more economically as

$$\mathbf{x} = \mathbf{Mf} \tag{3}$$

where the $(n \times 1)$ column vector $\mathbf{x}$ is the multispectral signal for a pixel (r values), $\mathbf{f}$ is the $(m \times 1)$ vector of endmember frequencies (q values), and $\mathbf{M}$ is the endmember spectral matrix such that the jth column of $\mathbf{M}$ is the spectra of the jth endmember (a values). Because $\mathbf{x}$ and $\mathbf{M}$ are known, provided there are as many equations as unknowns ($m \leq n$), the system can be solved for $\mathbf{f}$ (i.e., $q_1, q_2, \ldots, q_m$). If $n > m$, the expressions in Eq. 2 can also include an error term because inconsistent solutions could arise from measurement errors and deviations from model assumptions; that is, attempting to solve for $\mathbf{f}$ will result in contradictory mathematical statements. In this case, a least squares approach can be used to estimate $\mathbf{f}$ in a manner that comes closest to satisfying all the equations overall (Shimabukuro and Smith 1991). However, the procedure outlined here is naïve in that it does not generate a least squares approximation. Instead, when $n > m$, the inconsistencies in the expressions of Eq. 2 are considered not as errors but as the effect of water depth. Depth is resolved by trying to find a depth at which the modified expressions of Eq. 2 are as consistent as possible. How this is done in practice will be described in stage 4, after it is shown how the effect of depth can be incorporated in the linear mixing model.

The effect of water depth on spectral mixing—The effect of depth on the apparent reflectances of the substrate can be expressed by applying Eq. 1 to each band in which **x** (the multispectral signal for each pixel) is measured. Using matrices, this can be accomplished by constructing $\mathbf{V}_z$ as an ($n \times n$) diagonal matrix containing values e^{-2k_1z}, e^{-2k_2z}, . . . , e^{-2k_nz}, where k_1, k_2, . . . , k_n are the diffuse attenuation coefficients corresponding to the spectral bands in which **x** is measured. Then

$$\mathbf{x}_z = \mathbf{V}_z\mathbf{x} = \mathbf{V}_z\mathbf{M}\mathbf{f} \tag{4}$$

where $\mathbf{x}_z$ is how material with reflectance **x** would actually appear with an interceding depth of water z (i.e., $\mathbf{x}_z$ is the apparent reflectance at depth z). Note from the above equation that $\mathbf{V}_z$ and the matrix of endmember spectra **M** can be combined into a depth-dependent endmember matrix, $\mathbf{M}_z = \mathbf{V}_z\mathbf{M}$. For a given depth z, the values of $\mathbf{M}_z$ express how the individual pure endmembers would appear at that depth. A modified version of Eq. 3 can now be written that makes explicit the role of water depth.

$$\mathbf{x}_z = \mathbf{M}_z\mathbf{f} \tag{5}$$

Conceptually, this expresses the idea that the measured reflectance of a substrate in a pixel at depth z can be considered a linear sum of the endmember reflectance spectra as they would appear at that depth themselves. This is equivalent to a set of simultaneous equations of the same form as Eq. 2, but where the a values have been modified by

$$a_{ij} \rightarrow e^{-2k_iz}a_{ij} \tag{6}$$

If there are more equations than unknowns ($n > m$), then to find z, note that when z is correct, all these equations must be true. The degree of inconsistency for incorrect values of z might not be immediately apparent, but the tests we have conducted (which are detailed later) indicate that it is sufficient to resolve z. A method for finding the correct value of z from the set of equations defined by Eq. 5 is explained next.

Gaussian elimination and estimation of depth—Using the principles of Gaussian elimination (Sedgewick 1988), the set of equations given by Eq. 5 can be reduced to a set of functions of z that will all equal zero when those equations are consistent and nonzero otherwise. By subtracting a multiple of the first equation in Eq. 2 from the remaining equations, a new set of $n - 1$ equations can be generated with no term in q_1. This procedure can be repeated with the new set of equations to remove the terms in q_2. After m repetitions, there are $n - m$ equations left with no q values at all, but instead with zero equated to an expression on the left-hand side which is composed of r values (the measured reflectance for the pixel), a values (the endmember spectra at depth zero), and terms of the form e^{-2k_1z}. Because all values apart from z are known, these functions—denoted $f_1(z)$, $f_2(z)$, . . . , $f_{n-m}(z)$—can form the basis for resolving z. The mathematical structure of these functions is complex, and they cannot be rearranged easily to give z directly. In practice, a successive approximation technique can give an estimate of z to the required level of accuracy. In principle, any of $f_1(z)$, $f_2(z)$, . . . alone could be used to find z. In practice, especially with introduced error, individual functions occasionally give multiple solutions for z or no solution at all. This situation can be resolved by considering two or more of the functions simultaneously. A practical method for obtaining the estimate of z from these functions is described next.

Estimation of z *by successive approximation*—The problem of finding z has been reduced to that of finding the value of z for which a set of functions $f_1(z)$, $f_2(z)$, . . . are all equal to zero. This can be achieved by systematically taking values of z to search for the points at which $f_1(z) = 0$, $f_2(z) = 0$, . . . , etc. It is most efficient to restrict z to the valid range of depths (i.e., $z_{min} \leq z \leq z_{max}$) where z_{min} will be zero and z_{max} should be slightly larger than the expected maximum depth at the site.

To find the roots of one function $f(z)$, start with a number of values at regular intervals between z_{min} and z_{max} and evaluate $f(z)$ at each of these points. Intervals within which there is a root $f(z) = 0$ have on one side $f(z) > 0$ and on the other side $f(z) < 0$. Such intervals can be subdivided into two new intervals half the size of the original and the process repeated. By this method, an estimate of z for which $f(z) = 0$ can be determined to the required level of accuracy. This approach does potentially miss intervals that initially contain two roots, but in practice, this has not proved significant and, in any case, can be combated by taking more intervals in the first instance. Some asymptotes also will be misidentified as roots by this scheme, but this may be solved by noting that as the intervals are subdivided, the values of $f(z)$ do not tend toward zero, but rather become increasingly large.

Each of $f_1(z)$, $f_2(z)$, . . . might exhibit several roots within the valid range, but in practice, incorrect roots are not replicated in more than one function. The majority of ambiguities as to the true estimate of z can be resolved by considering only $f_1(z)$ and $f_2(z)$ and taking the average of their closest two roots. In cases where multiple roots are found in only one of $f_1(z)$ or $f_2(z)$ and no roots are found in the other, the average of the location of the roots of the one can be taken. There is still the potential for cases where no solution for z is found. The extent to which this occurs is assessed later. In the next section is described an optional transform to concentrate the useful information into the first two functions $f_1(z)$ and $f_2(z)$, which enhances the performance of this approach.

Enhancement by principal components analysis—The following steps can be incorporated into the analysis to ensure that the maximum separability in the data is being exploited and to reduce the processing overhead when the number of bands greatly exceeds the number of endmembers. These procedures are entirely optional, and the technique can be performed without them.

The reflectance spectra of the m endmembers can be thought of as points in n-dimensional space, where the position of the point on the ith axis is the spectral signal in that band. Taken this way, it is easy to see the redundancy of information when few endmembers are measured in many bands. For example, three separable endmembers in n-dimensional space will form a triangle in a 2-dimensional plane regardless of the value of n (provided $n > 2$). Linear

mixtures of those three endmembers will lie within the triangle in the same plane. Performing a PCA on the endmember spectra projects the points in space so that the first two new axes (or bands) describe the plane of that triangle.

In general then, a useful transform is to perform a PCA on the columns of **M** in order to extract $m - 1$ bands, which will encompass the separability of the m endmembers. The initial step of standardizing the means and variances of the variables, customary with PCA (Manly 1994), is unnecessary. The transform is performed by constructing the matrix **A** such that its rows are the eigenvectors of the covariance matrix of **M**, ordered such that the corresponding eigenvalues decrease in magnitude (Manly 1994). Then Eq. 5 can then be modified as

$$\mathbf{Ax} = \mathbf{AM}_z\mathbf{f} \tag{7}$$

The linear mixture model still holds if the set of endmembers and the measured spectral signal are pretransformed by the same matrix. The matrix **A** is calculated once from the set of endmember spectra and then applied to the spectral signal at every pixel. If $\mathbf{x}_p = \mathbf{Ax}$ and $\mathbf{M}_p = \mathbf{AM}_z$, then we can write

$$\mathbf{x}_p = \mathbf{M}_p\mathbf{f} \tag{8}$$

Equation 8 again defines a set of simultaneous equations of the form in Eq. 2. The first m equations encompass the variation required to unmix endmembers at depth 0. The subsequent $n - m$ equations will contain information when other factors such as depth or measurement error arise. The distribution of such information among these equations will be difficult to predict, so an optimum solution would order equations by their importance and confine processing to the first few. This is done by selecting a subset of variables and performing a PCA on those alone (again, without the initial standardization step), concentrating the variance into a smaller set of variables. Specifically, the PCA is performed on the $m + 1$ to n transformed variables for all the endmembers (i.e., the lower $n - m$ rows of $\mathbf{M}_p$). Let $b = n - m$ and construct **B** as the $(b \times n)$ matrix composed of the lower b rows of $\mathbf{M}_p$; then find the $(b \times b)$ matrix of eigenvectors of **B**'s covariance matrix. $\mathbf{A}_2$ is then the identity matrix in the first $n - b$ rows and columns and contains these eigenvectors in the final $n - b$ columns of the last $n - b$ rows. Then $\mathbf{M}_p \rightarrow \mathbf{A}_2\mathbf{M}_p$ will transform only the final b rows of $\mathbf{M}_p$. The first m equations defined by Eq. 8 with this new $\mathbf{M}_p$ are as before, but the subsequent $n - m$ equations contain decreasing amounts of information. Therefore, the first function of z produced from the Gaussian elimination contains the maximum information of use for resolving z.

Practical summary of the procedure

A practical step-by-step summary of the procedure is as follows.

1. If necessary, radiometrically convert the image to reflectance values and correct for atmospheric effects.
2. Obtain zero-depth reflectance spectra for all m endmembers in n wavelength bands. These should be arranged in the $(n \times m)$ matrix **M** such that the jth column of **M** is the spectra of the jth endmember. In practice, the endmember reflectance spectra can be obtained from a spectral library, in situ measurements, or depth-corrected regions of the image where the substrate and depth are known from ground truth data.
3. Obtain n diffuse attenuation coefficients $k_1, k_2, \ldots, k_n$ for the water at the site in the same wavelengths as the endmember spectrum bands. These can be measured directly at the site or inferred from image data if several pixels of the same substrate can be identified at a range of known depths.
4. If $n > m + 2$, evaluate the eigenvectors according to a PCA on the endmember matrix **M**. The usual step of standardizing each variable to a mean of zero and unit variance is omitted. The matrix **A** is constructed from the eigenvectors $\mathbf{a}_1, \mathbf{a}_2, \ldots, \mathbf{a}_n$ ordered by decreasing eigenvalue such that the ith row of **A** is $\mathbf{a}_i$. No data are actually transformed at this stage.

For each pixel, the following steps must be repeated for successive estimates of depth, z_{est}. In essence, they describe how to evaluate the functions $f_1(z_{est}), f_2(z_{est}), \ldots, f_{n-m}(z_{est})$.

5. For an estimate of depth z_{est}, derive the set of endmembers as they would be expected to appear at that depth, $\mathbf{M}_z$, from **M** by Eq. 4.
6. If **A** has been constructed as described above, then transform the at-depth endmember spectra and the spectral signal **x** into the ''space'' of the PCA by $\mathbf{M}_p = \mathbf{AM}_z$ and $\mathbf{x}_p = \mathbf{Ax}$. Alternatively, these can be used as they are (i.e., $\mathbf{M}_p = \mathbf{M}_z$ and $\mathbf{x}_p = \mathbf{x}$).
7. An additional optional step that improves the performance of the technique is to apply a PCA to the m to n rows of $\mathbf{M}_p$ and similarly transform $\mathbf{x}_p$. Those rows alone are transformed by the matrix of resulting eigenvectors sorted by decreasing eigenvalue.
8. The linear mixing model $\mathbf{x}_p = \mathbf{M}_p\mathbf{f}$ defines a set of n simultaneous equations in m unknowns (the values of **f**). The equations defined by the first m rows of $\mathbf{M}_p$ can be used to eliminate the terms in **f** from the equations defined by the remaining $(n - m)$ rows of $\mathbf{M}_p$. If this elimination is performed, the remaining constants are the values of $f_1(z_{est}), f_2(z_{est}), \ldots, f_{n-m}(z_{est})$.
9. By repeating from step 5, the roots $f_1(z_{est}) = 0$, $f_2(z_{est}) = 0, \ldots$ can be determined and an estimate of the actual depth z obtained from them, as described in stage 5 of the outline.

Once the depth has been estimated for the pixel, the spectral signal **x** can be depth corrected to $\mathbf{x}_c$ by the inverse of Eq. 1. Classical spectral unmixing can then proceed by the estimation

$$\mathbf{f} = \mathbf{M}_t^{-1}(\mathbf{x}_c)_t \tag{9}$$

where the subscript t indicates that $\mathbf{M}_t$ is the $(m \times m)$ matrix composed of the first m rows of **M**, and $(\mathbf{x}_c)_t$ is the first m values of $\mathbf{x}_c$. A sounder method, which utilizes all of the variance in the endmembers, is given by

$$\mathbf{f} = (\mathbf{AM})_t^{-1}(\mathbf{Ax}_c)_t \tag{10}$$

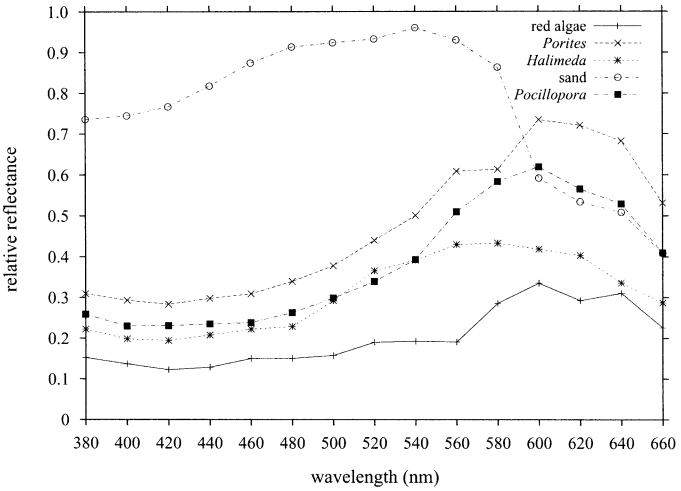

Fig. 1. Endmember spectra.

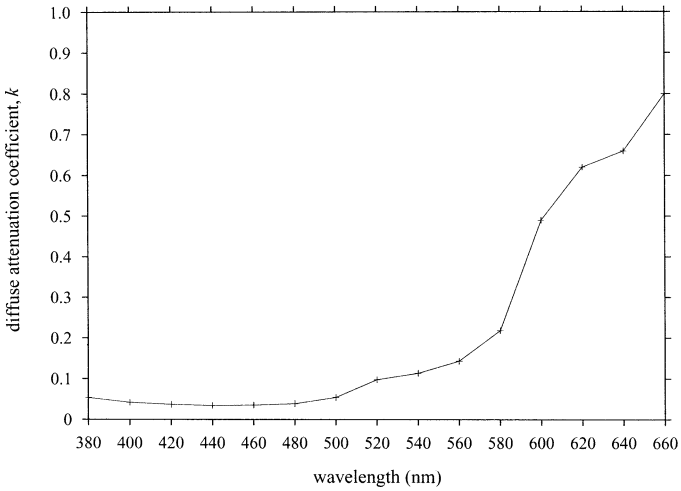

Fig. 2. Water diffuse attenuation coefficients.

Implementation details

Despite the apparent computational complexity of the method, efficient implementation is possible by quantizing the depth range into small discrete intervals. The bulk of the calculations can then be performed in a preprocessing step specific to these depths. Quantizing depth into 1,000 intervals over a depth range of 10 m gives an inherent upper limit of 0.005 m to the accuracy of depth estimation (each interval is 0.01 m, so an estimate in the center of the correct interval is, at most, 0.005 m in error). An inherent error of 0.005 m is very small compared to the inaccuracy introduced by other sources of error (*see the next section*). The matrices $\mathbf{M}_z$ and $\mathbf{M}_p$ and the forward transform for Gaussian elimination can then be calculated for each discrete depth prior to image analysis. The most intensive calculations required in this preprocessing step are the determination of the eigenvectors for the PCA transform. On a typical workstation, the preprocessing step for five endmembers in 15 bands with 1,000 depth intervals takes approximately 10 s. Subsequent analysis of 100,000 pixels takes approximately 30 s (equivalent to 90 km^2 of satellite image at 30 $\times$ 30-m pixel resolution).

Experimental test

The robustness of the technique toward various sources of error was tested using a model. Spectral data in 15 bands were simulated for random mixtures of five endmembers, at random depths between 0 and 10 m according to linear mixing and Eq. 1. The depth/unmixing technique was then applied to analyze the simulated spectra. In one set of trials, the endmember reflectance spectra were generated randomly for each repeat, with each spectrum consisting of 15 spectrally uncorrelated reflectance values drawn from a uniform distribution between zero and one. A second set of trials used the realistic spectra of five benthic components of coral reefs between 380 and 660 nm (Fig. 1). These ''realistic spectra'' are from a library of reef spectra measured in situ (P.J.M. unpubl. data; *see* Clark et al. 2000 for collection details). Some spectra have been rescaled because their relative magnitude in the raw data was found not to be in realistic proportion to the others (this rescaling will not affect the behavior of the technique). Realistic values for water diffuse attenuation coefficients were used in both cases, being set as twice those published for the clearest natural waters (Fig. 2; Smith and Baker 1981). Values of this order have been reported on coral reefs (Maritorena and Guillocheau 1996). Valid estimates of depth were restricted to the range $-2 < z < 12$, so as not to exclude estimates that fell only slightly outside the true range.

Error was introduced into the model in three ways.

1. *Sensor error.* Error on the spectral signal **x** was incorporated by adding a different random value to each term in the vector **x**. The added values are normally distributed, zero centered, and spectrally uncorrelated (i.e., like random noise). The magnitude of the added values (i.e., the range of the normal distribution from which they are taken) is expressed in relation to the magnitude of the original value to which they are being added. For example, 10% sensor error implies that the error being added on each term comes from a normal distribution with a standard deviation that is half of 10% of the original value of the term. That is, a 10% sensor error implies a positive or negative error, which in 95% of cases is within 10% of the true value. In practice, this form of error could result from uneven behavior of the sensor over an image.
2. *Endmember error.* A normally distributed error was added to each value in **M**. The error terms are derived as described in the previous section, being taken from a normal distribution with a standard deviation half the given proportion of the true value. The modified **M** was used in the analysis, whereas the original true **M** was used to construct the spectral signal. Such errors would arise from inaccurate measurements of endmembers and spatial changes in endmember spectra (e.g., intraspecific variation in reflectance).
3. k-*Value error.* Water quality can vary within a site, and the accurate measurement of diffuse attenuation coefficients can be problematic, especially if estimated from an

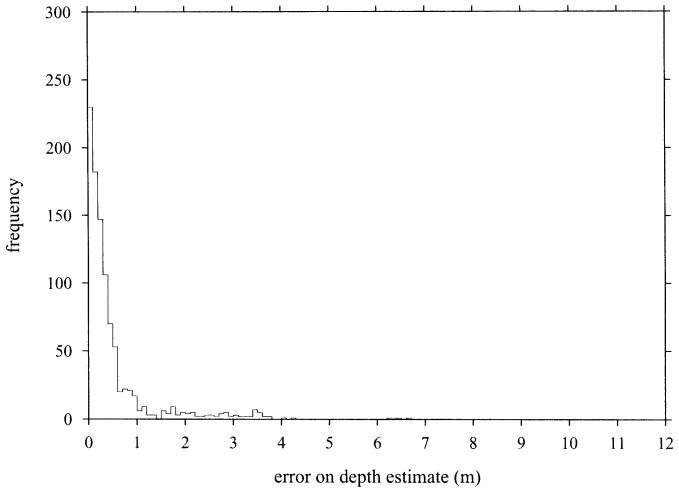

Fig. 3. Error on depth estimates with 10% sensor error only; 87% of estimates within 1 m of accuracy.

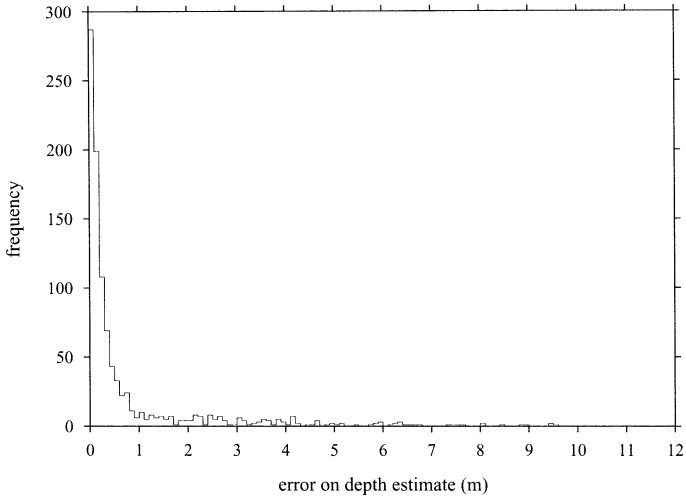

Fig. 4. Error on depth estimates with 10% endmember error only; 81% of estimates within 1 m accuracy.

image. To assess the performance under this kind of error, a term equivalent to a measurement error on the water diffuse attenuation coefficients was added in the same way as described in (1) above. Original values were used to generate the mixed pixel; the values with error were used in the analysis.

The technique was applied for nine runs of 1,000 simulations, with each run having a different combination of introduced errors. Sensor errors, endmember errors and *k*-value errors of 0, 5, and 10% were included in the following combinations: (0, 0, 0); (5, 0, 0); (0, 5, 0); (0, 0, 5); (5, 5, 5); (10, 0, 0); (0, 10, 0); (0, 0, 10); (10, 10, 10). The nine error conditions were performed with real and random endmembers. A final run with real endmembers and 20% error on all three terms gave a total of 19 experimental runs. Note that because of the large number of values to which error is added in each simulation, the probability of at least some large errors is high. For example, under conditions of 20% error on all three terms, errors are added to 5×15 values in the endmember spectra, 15 *k*-values, and the 15 values of the spectral signal—a total of 105 values. Under conditions of 20% error on all three terms, the definition of percent error used implies that every simulation will contain on average five values that are at least 20% in error and approximately 37 values that are >10% in error. Similarly, even when only sensor error or *k*-value error is introduced (affecting only 15 values), the chances that at least one value will be in error by an amount greater than the defined percent error is better than even (the probability being $1 - 0.95^{15} = 0.54$).

The accuracy of depth estimations was gauged by the percentage of estimations falling within 1 m of the true value (which is 10% of the total depth range of 0–10 m). Assessment of absolute errors is preferable to using a percent error of the actual depth because percent error becomes very large when depth becomes small (tending to infinity for any error at all as depth tends to zero). Unmixing accuracy was assessed in a similar way by calculating the mean of the errors on the estimated endmember proportions. The method of using the average error on the proportion estimates was selected as being both a simple and an intuitive approach to assessing unmixing accuracy. The average error ranges from zero (all estimates correct) to unity for a worst-case scenario, where a pixel composed entirely of one pure endmember is classified as being composed of another pure endmember. Kolmogoroff–Smirnoff tests (with Dunn–Šidák correction to the α level, Sokal and Rohlf 1995) were used to detect whether the distribution of errors differed between the conditions. The performance with random and real spectra was compared under each condition of introduced error. Finally, to determine whether there was any depth-dependent effect on the accuracy of depth estimates, the depth estimate error and actual depth were recorded for 1,000 simulations under medium error conditions (with real endmembers and 5% error in all three terms).

Results

In 16 of the 19 experimental conditions, the technique found a solution for depth in more than 99% of simulations. In the remaining three conditions (real endmembers with 10% sensor error alone and with 10% and 20% error on all three terms), slightly less than 98% of simulations were able to resolve depth. This indicates a relatively high sensitivity of the technique to sensor error as opposed to either endmember or *k*-value errors.

The accuracy of depth estimates where realistic endmembers were used with a 10% sensor, endmember, and *k*-value error are shown in Figs. 3–5, respectively. For a depth range of 10 m, 87% of the depth estimates were within 1 m when 10% sensor error was introduced (Fig. 3). Depth errors were greater when a comparable endmember error was introduced (81% within 1 m, Fig. 4) but similar to *k*-value error (88% of estimations within 1 m, Fig 5). Kolmogoroff–Smirnoff tests confirmed that the distribution in Fig. 4 differed significantly from those in Figs. 3 and 5 (in both cases, $P < 0.001$), but the latter did not differ significantly from each other ($P = 0.055$). When 10% errors were introduced from

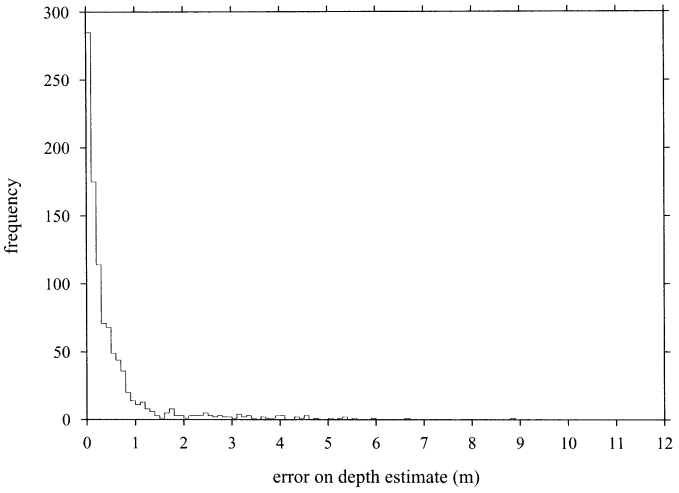

Fig. 5. Error on depth estimates with 10% *k*-value error only; 88% of estimates within 1 m of accuracy.

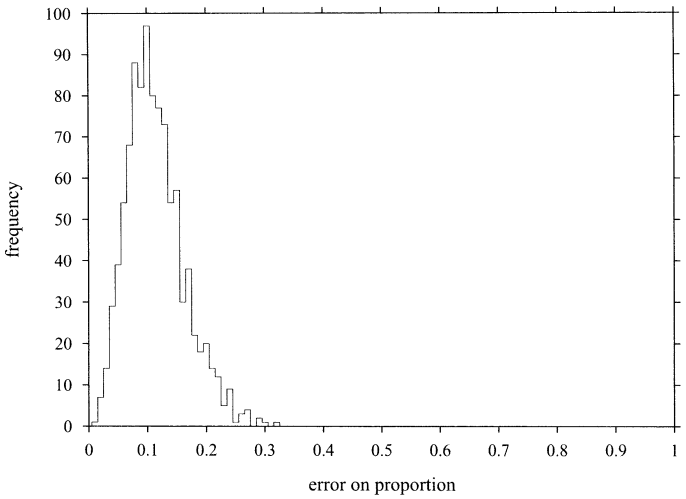

Fig. 7. Error on endmember proportion estimates with 5% measurement error, 5% endmember error, and 5% *k*-value error.

all three sources, only 65% of depth estimates were within 1 m (Fig. 6). However, whereas these introduced errors had a moderate effect on depth estimates, their effect on the estimation of endmember quantities was relatively small. With 5% errors introduced into all three terms, 90% of simulations had an average error on the endmember proportions of <0.18 (Fig. 7). When a 20% error was introduced to all three terms, 53% of depth estimates were within 1 m and the average error on the endmember proportions was <0.21 in 90% of cases.

A further nine α-corrected Kolmogoroff–Smirnoff tests were performed to detect differences between the conditions of real and random endmember spectra. The distribution of errors on the depth estimates with no introduced error showed no significant difference ($P = 0.18$) between the realistic and random conditions (in both cases, there was no error on the depth estimates for all 1,000 simulations). With any error source of 5 or 10%, the technique performed significantly differently with random than with realistic endmembers, (in all cases, $P < 0.001$). In fact, the overall accuracy was somewhat better with realistic spectra, random spectra giving only 73% of depth estimates within 1 m with 10% sensor error and 79 and 73% for comparable endmember and *k*-value errors, respectively. It is interesting to note that the condition in which realistic endmembers fared worse (on endmember error) was the most accurate with random endmembers.

To ascertain whether there was any depth-dependent effect on the accuracy of depth estimates, a frequency histogram of the average error in depth estimates was plotted against actual depth for one run (with real endmembers and 5% error in all three terms, Fig. 8). The slight bimodal aspect of this chart is an inevitable artifact of the analysis: because the method only looks for depth estimates in the range -2 to 12 m, actual depths at the extreme ends (close to 0 or 10

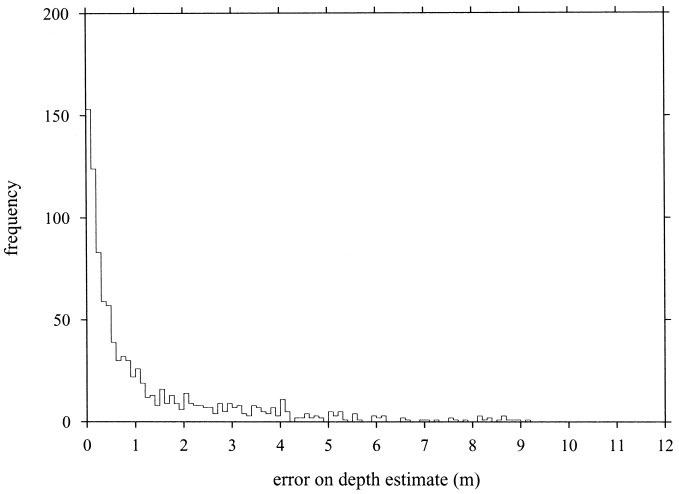

Fig. 6. Error on depth estimates with 10% measurement error, endmember error, and *k*-value error; 65% of estimates within 1 m of accuracy.

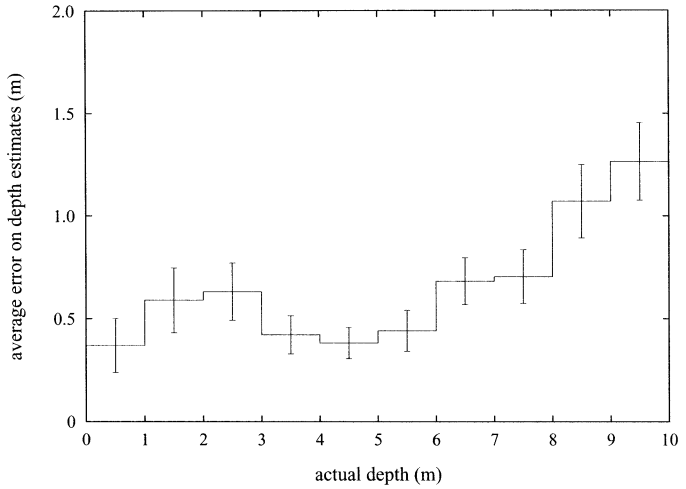

Fig. 8. Average error on depth estimates as a function of depth from a run with 5% measurement error, 5% endmember error, and 5% *k*-value error. Error bars represent ± 1 SE on the mean of depth estimate errors.

m) can produce physically larger estimate errors (≤12 m) than those in the middle (for an actual depth of 5 m, the maximum estimate error is 7 m). However, despite this artifact, there is a clear depth-dependent effect in the accuracy of depth estimates. Errors increase for greater depths, with an average error of >1 m at depths of 9–10 m, compared to <0.5 m in the range 0–1 m (Fig. 8).

Discussion

Although the formulation of the technique gives a solution for *z* defined precisely in mathematical terms, it was not initially clear how robust its performance would be when errors of the kind found in real data were introduced. It was possible that these inconsistencies could result in many failures to find a solution for *z* or wildly inaccurate values for solutions that were found. On the contrary, testing has shown that, with realistic data, the technique is robust against modest errors (i.e., 80% of depth estimates were within 1 m when various sources of error were introduced).

The sensitivity of the method was actually slightly better for real coral reef spectra than for random spectra, which gave a similar distribution of errors but with a wider range. As regards numerical input to the technique, these real spectra perform slightly better than could be expected at random. This observation is encouraging because the spectral differences between reef substrata (which in this case included two coral genera) can be subtle (Holden and LeDrew 1998; Clark et al. 2000). Importantly, 90% of the unmixing of endmember proportions was accurate to within 0.18 (of the possible range 0–1), with moderate introduced errors, and within 0.21 even under conditions of the most introduced errors (20% on all three terms). Errors on the depth estimates that are somewhat larger under this condition (only 53% of estimates were within 1 m) implies that, under the model used here, spectral unmixing is fairly insensitive toward errors in the depth estimation. Again, this result is encouraging for the use of spectral unmixing when mapping benthic substrata in aquatic systems.

The application of the technique to field data requires several caveats. Like spectral unmixing in terrestrial systems, the technique fails if the endmember spectra do not mix linearly (i.e., if the spectral mix does not equal the spatial mix of endmembers). In this case, however, such nonlinearity disrupts both the estimation of depth and endmember quantities. A second potential problem is the existence of unknown endmembers. However, simulations indicate that the technique is robust against a finite number of unknown endmembers mixing in small fractions because such effects would be similar to the sensor errors introduced here.

Simulations suggest that the error in depth estimates increases as depth increases. As depth increases, the spectral signal from the benthos becomes more attenuated, so noise in the sensor (and from other sources) will increasingly mask the information that can be resolved. Although increased water clarity would improve the depth range over which the method could be applied, attenuation must occur in some bands in order for depth to be calculated. For example, spectral bands in the wavelength region of least attenuation (e.g., ~400–500 nm in the clearest natural waters, Smith and Baker 1981) alone might not contain sufficient information to resolve depth. For maximal applicability over a range of depths, a selection of spectral bands with differing attenuation in water should be chosen.

Currently, the method as outlined is best suited for application to airborne hyperspectral remotely sensed data (e.g., from CASI or AVIRIS). The majority of satellite sensors do not record in a sufficient number of spectral bands, the absolute minimum requirement being the number of endmembers plus two. However, this situation is likely to change in the future (e.g., with the recent launch of the Hyperion hyperspectral sensor). Radiometric correction of the remotely sensed signal would be beneficial, and possibly necessary, if the method is to be applied to satellite sensed data.

One strength of the technique is that it is not necessarily dependent on any particular model of light attenuation in water. As long as the model used can be characterized in every parameter other than depth, then depth remains the single variable to be solved for. For example, backscatter can be incorporated by using the equation (Bierwirth et al. 1993)

$$R_d = R_0 e^{-2k_i z} + R_W(1 - e^{-2k_i z}) \quad (11)$$

where R_W is the apparent reflectance of deep water in band *i*. As long as the spectral signal of deep water (values of R_W) is known, this can be used in place of Eq. 1 to modify the endmember spectra. The incorporation of backscatter is potentially very important because under most circumstances where the bottom is deeper than a few meters, the backscatter term can no longer be neglected even in clear waters (Philpot 1987; Lee et al. 1994). A priority for future investigation is whether incorporating backscatter will have an effect on the dynamics of the technique.

The technique can also be improved by incorporating the possibility of variation in endmember spectra. The current formulation assumes that each endmember can be represented by a single ''ideal'' reflectance spectrum. In practice, a single endmember will exhibit variation around a mean spectrum. Corals, for example, exhibit intraspecific variation in reflectance spectra (Clark et al. 2000). Currently, all variation outside of that which can be explained as linear mix of idealized endmembers is utilized to resolve depth (and hence assumed to be the result of depth). An improved method would partition the variation that is accountable by variation in endmembers from that which should be attributed to depth. This would give a greater degree of freedom to the model and hence affect the ability to resolve depth negatively. However, a least squares approximation technique based on this approach (Shimabukuro and Smith 1991) might be more accurate and robust overall.

References

ADAMS, J. B., M. O. SMITH, AND P. E. JOHNSON. 1986. Spectral mixture modelling: A new analysis of rock and soil types at the Viking Lander I site. J. Geophys. Res. **91:** 8098–8112.

BENNY, A. H., AND G. J. DAWSON. 1983. Satellite imagery as an aid to bathymetric charting in the Red Sea. Cart. J. **20:** 5–17.

BIERWIRTH, P. N., T. J. LEE, AND R. V. BURNE. 1993. Shallow sea-

floor reflectance and water depth derived by unmixing multispectral imagery. Phot. Eng. Remote Sens. **59:** 331–338.

BROWN, M., S. R. GUNN, AND H. G. LEWIS. 1999. Support vector machines for optimal classification and spectral unmixing. Ecol. Model. **120:** 167–179.

CLARK, C. D., P. J. MUMBY., J. R. M. CHISHOLM, J. JAUBERT, AND S. ANDRÉFOUËT. 2000. Spectral discrimination of coral mortality states following a severe bleaching event. Int. J. Remote Sens. **21:** 2321–2327.

FOODY, G. M., AND D. P. COX. 1994. Sub-pixel land cover composition estimation using a linear mixture model and fuzzy membership functions. Int. J. Remote Sens. **15:** 619–631.

GREEN, E. P., P. J. MUMBY, A. J. EDWARDS, AND C. D. CLARK. 1996. A review of remote sensing for the assessment and management of tropical coastal resources. Coast, Manag. **24:** 1–40.

———, ———, ———, AND ———. 2000. Remote sensing handbook for tropical coastal management. UNESCO.

HOLDEN, H. M., AND E. F. LEDREW. 1998. The scientific issues surrounding remote detection of submerged coral ecosystems. Prog. Phys. Geogr. **22:** 190–221.

JUPP, D. L. B. 1988. Background and extensions to depth of penetration (DOP) mapping in shallow coastal waters, p. IV.2.1–IV.2.19. *In* Proceedings of the International Symposium on Remote Sensing of the Coastal Zone, Gold Coast, Queensland.

KIMES, D. S., J. A. SMITH, AND K. J. RANSON. 1980. Vegetation reflectance measurements as a function of solar zenith angle. Phot. Eng. Remote Sens. **46:** 1563–1573.

LEDREW, E., H. HOLDEN, D. PEDDLE, J. MORROW, R. MURPHY, AND W. BOUR. 1995. Towards a procedure for mapping coral stress from SPOT imagery with in situ optical correction, p. 211–219. *In* Proceedings of the 3rd Thematic Conference on Remote Sensing of the Marine Coastal Environment. V. 1.

LEE, Z., K. L. CARDER, S. K. HAWES, R. G. STEWARD, T. G. PEACOCK, AND C. O. DAVIS. 1994. Model for the interpretation of hyperspectral remote-sensing reflectance. Appl. Opt. **33:** 5721–5732.

———, ———, R. F. CHEN, AND T. G. PEACOCK. 2001. Properties of the water column and bottom derived from Airborne Visible Infrared Imaging Spectrometer (AVIRIS) data. J. Geophys. Res. **106:** 11,639–11,651.

LYZENGA, D. R. 1978. Passive remote sensing techniques for mapping water depth and bottom features. Appl. Opt. **17:** 379–383.

MANLY, B. F. J. 1994. Multivariate statistical methods, 2nd ed. Chapman & Hall.

MARITORENA, S., AND N. GUILLOCHEAU. 1996. Optical properties of water and spectral light absorption by living and non-living particles and by yellow substances in coral reef waters of French Polynesia. Mar. Ecol. Prog. Ser. **131:** 245–255.

MATHER, P. M. 1999. Computer processing of remotely-sensed images, 2nd ed. Wiley.

MOBLEY, C. D. 1994. Light and water. Academic.

MUMBY, P. J., J. R. M. CHISHOLM, C. D. CLARK, J. D. HEDLEY, AND J. JAUBERT. 2001. A bird's-eye view of the health of coral reefs. Nature **413:** 36.

NORDMAN, M. E., L. WOOD, J. L. MICHALEK, AND J. J. CHRISTY. 1990. Water depth extraction from Landsat-5 imagery, p. 1129–1139. *In* Proceedings of the 23rd International Symposium on Remote Sensing of the Environment.

PEDDLE, D. R., E. F. LEDREW, AND H. M. HOLDEN. 1995. Spectral mixture analysis of coral reef abundance from satellite imagery and in situ ocean spectra, Savusavu Bay, Fiji, p. 563–575. *In* Proceedings of the 3rd Thematic Conference on Remote Sensing of the Marine Coastal Envirnoment. V. 2.

PHILPOT, W. D. 1987. Radiative-transfer in stratified waters—a single scattering approximation for irradiance. Appl. Opt. **26:** 4123–4132.

SEDGEWICK, R. 1988. Algorithms, 2nd ed. Addison-Wesley.

SHIMABUKURO, Y. E., AND J. A. SMITH. 1991. The least-squares mixing models to generate fraction images derived from remote sensing multispectral data. IEEE Trans. Geogr. Remote Sens. **29:** 16–20.

SMITH, R. C., AND K. S. BAKER. 1981. Optical properties of the clearest natural waters. Appl. Opt. **20:** 177–184.

SOKAL, R. R., AND F. J. ROHLF. 1995. Biometry, 3rd ed. Freeman.

Received: 21 August 2001
Amended: 3 December 2001
Accepted: 2 January 2002